crystals

MDPI

Article

A Novel Nanostructured Mullite Feedstock for Environmental Barrier Coatings via Atmosphere Plasma Spraying

Fei Xiao [1,2], Xue Gong [3], Saiyue Liu [4], Jin Jia [1], Xiaodong Zhang [1,*], Lan Wang [1], Mufu Yan [1] and You Wang [1]

[1] School of Materials Science and Engineering, Harbin Institute of Technology, Harbin 150001, China; 042320020@163.com (F.X.); jiajin@hit.edu.cn (J.J.); 13206552160@163.com (L.W.); yanmufu@hit.edu.cn (M.Y.); wangyou@hit.edu.cn (Y.W.)
[2] Liaoning Research Institute of Light Industry, Shenyang 110036, China
[3] College of Aerospace Engineering, Shenyang Aerospace University, Shenyang 110136, China; gongxue_hit@163.com
[4] Space Environment Simulation Research Infrastructure, Harbin Institute of Technology, Harbin 150001, China; yueyuedeyouxiang123@126.com
* Correspondence: zhangxiaodong@hit.edu.cn; Tel.: +86-451-8640-2710

Abstract: A novel strategy is proposed to design an exclusive nanostructured mullite spherical feedstock for environmental barrier coatings (EBCs) via atmosphere plasma spraying (APS). The nanostructured mullite spherical feedstocks are successfully obtained by the procedure of spray drying, solid-phase sintering and flame spheroidization. The crystal grain size of nano-mullite increases with annealing temperature. When the temperature is as high as 1500 °C, the reaction of Al_2O_3 and SiO_2 can be fully completed. The average size is 52 nm for the grain of mullite in feedstocks sintered at 1500 °C, which can be reduced from 52 nm to 48 nm by flame spheroidization treatment as well. Meanwhile, the nanostructured spherical feedstocks show high density and good flowability, which is suitable for APS. The mullite coatings is successfully prepared on a SiC substrate by APS, in which both the nanoscale crystals and nanostructures are perfectly kept as designed. Furthermore, there is no crack appeared in the nanostructured mullite coatings. Thus, the nanostructured mullite feedstock is one of promising candidates for the high performance EBCs.

Keywords: nanostructured mullite; feedstocks; plasma spraying; environmental barrier coatings

Citation: Xiao, F.; Gong, X.; Liu, S.; Jia, J.; Zhang, X.; Wang, L.; Yan, M.; Wang, Y. A Novel Nanostructured Mullite Feedstock for Environmental Barrier Coatings via Atmosphere Plasma Spraying. *Crystals* **2022**, *12*, 726. https://doi.org/10.3390/cryst12050726

Academic Editors: George D. Verros and Dah-Shyang Tsai

Received: 2 March 2022
Accepted: 12 May 2022
Published: 19 May 2022

1. Introduction

Due to their low density and high-temperature stability, silicon-based ceramic materials are excellent candidate materials for hot components of next-generation aviation engines and gas turbines [1–4]. In the dry oxygen atmosphere, a protective SiO_2 layer is formed on the surface of silicon-based ceramics, which is the reason for its excellent oxidation resistance. However, SiO_2 layer reacts with vapor water to form volatile $Si(OH)_4$, resulting in corrosion failure of such silicon-based ceramics. In addition, calcia-magnesia-alumino-silicate (CMAS) corrosion is another urgent problem that needs to be solved when silicon-based ceramics are used as aviation engine components [5–7]. These two disadvantages have limited the application of silicon-based ceramics in next-generation aviation engines and gas turbines. Environmental barrier coatings (EBCs) have been proposed to improve the corrosion resistance of ceramic components [1,8].

At present, many material systems have been developed for EBCs [9,10]. The current third generation of the EBC system is composed of a silicon bond coat, an intermediate diffusion barrier layer of mullite ($Al_6Si_2O_{13}$), and a top layer of rare earth silicates ($RE_2Si_2O_7$ or RE_2SiO_5) [11–13]. Among them, the mullite layer plays a crucial role in mitigating thermal mismatch and antioxidant activity. Mullite is very attractive due to its high melting temperature (1828 ± 10 °C), high refractoriness, and close thermal expansion coefficient to silicon-based ceramics [14–18]. Atmospheric plasma spraying (APS) is one of the most

widely used methods for preparing the EBCs. The studies have found that the cracks, pores and splats are the inherent characteristics of plasma-sprayed coatings [7,15,19–21]. The fine cracks and pores can play a role of channels for releasing stress. However, the water vapor and CMAS can penetrate into the mullite interlayer through the vertical cracks and pores, thereby causing an accelerated oxidation and corrosion at the interface between Si bond coat and mullite. The severe oxidation and corrosion will result in the spalling and failure of the EBCs, which is detrimental to the service life and reliability of the aero-engine. Therefore, it is critical to control the number of defects in the plasma sprayed coating.

In order to solve these problems, different methods have been attempted in recent years. One is to adjust the thermal spraying parameters. S. Latzel et al. [20] prepared mullite coating by APS. The results shown that the porosity can be reduced by reducing the spraying distance, increasing the carrier gas flow or changing the gas flow. However, the reduction of these spraying parameters induced the formation of a cracked layer usually. The research indicated the effect of improve the quality of the coatings only by adjusting the plasma spraying parameters is limited. The grain size, density and flowability of the feedstocks are another important factor affecting the quality of the coatings [22,23]. Many studies have found that the properties of coating prepared by nanostructured feedstocks are better than that of microstructured feedstocks [8,21,24]. The nanostructured coatings can reduce the thermal conductivity and cracks in the coatings, which is beneficial to improve the adhesive strength, corrosion resistance, thermal shock resistance, etc. [25–28]. The coatings prepared by nanostructured feedstocks maintain the characteristics of nano structure, which has high sintering resistance, fracture toughness and wear resistance [29,30]. It is a challenging problem to ensure that coatings prepared by nanostructured feedstocks maintain their nanostructure, which mainly depends on the design, regulation and preparation of feedstock.

However, a shortcoming of nanoparticle powders is that they cannot be successfully thermal sprayed due to their low mass and their inability to be carried in a moving gas stream and deposited onto a substrate. Additionally, the strong surface interaction of individual nanoparticles can lead to agglomeration in the process of powder feeding. Nanoparticle regranulation technology is one of effective methods to prepare the nanostructured feedstocks for plasma spraying [31,32]. Nanoparticle regranulation technology includes spray drying, sintering and even flame spheroidization. For the synthesis of nanostructured mullite feedstock, sintering is the heat treatment of the mixture of Al_2O_3 and SiO_2 nanopowders, which is the key process in regranulation. Flame spheroidization can further improve the density and flowability of the feedstocks. At present, the commercial mullite feedstocks formed by Al_2O_3 and SiO_2 powders are micron-sized. It is an urgent issue to develop nanostructured mullite feedstocks and ensure nanostructured characteristics of the coatings. However, there is no research report on the preparation and characterization of nanostructured mullite feedstocks for plasma spraying.

In this work, nanostructured mullite feedstocks were prepared by nanoparticle regranulation technology. The effect of sintering temperature on the content and grain size of mullite were investigated. The microstructure and phase composition of powders in different preparation stages were analyzed. The flowability, bulk density and tap density of nanostructured mullite feedstocks were tested. The microstructure and phase composition of coating prepared by nanostructured mullite feedstocks were also studied. This work is important to promote the practical application of EBCs in aviation engines and gas turbines.

2. Experimental

2.1. Materials

Nanostructured mullite feedstocks were prepared by using 71.83 wt.% Al_2O_3 (99.95%, 20 nm, Shanghai Kaiyin Chemical Co., Ltd., Shanghai, China), and 28.17 wt.% SiO_2 (99.95%, 20 nm, Ningbo Jinlei Nano Material Technology Co., Ltd., Ningbo, China) as raw materials. The mixture of Al_2O_3 and SiO_2 was mechanically activated in a planetary mill using distilled water, to which ammonium citrate dispersant (Sinopharm Chemical Reagent

Co., Ltd., Shanghai, China) and polyvinyl alcohol (Sinopharm Chemical Reagent Co., Ltd., Shanghai, China) were added. After milling, the mixture slurry was spray dried with a rotary atomizer spray dryer equipment LZG-15 (Wuxi Fenghua Drying Equipment Co., Ltd., Wuxi, China). The EBC coating was prepared with Si (20–50 μm, fused and crushed, 99.9% pure, Beijing Dadi Zelin Silicon Industry Co., Ltd., Beijing, China), and mullite feedstocks by APS.

2.2. Process

The mullite water suspension mixture with a 28.5 wt.% of solid content was prepared. To condition the suspensions, 1 wt.% of ammonium citrate dispersant and 0.2 wt.% of PVA binder were added. Thorough mixing of all ingredients was assured by using a planetary mill to avoid powder agglomeration.

The slurries were spray-dried with a rotary atomizer spray dryer equipment. The temperatures at inlet spray dryer change from 190 to 210 °C, while the ranged is from 80 to 100 °C at exit. The slurry was fed at 166 mL/min and 5×10^5 Pa of air pressure. The spray dried powders were sintered in the furnace (HT 64/17, Nabertherm GmbH, Germany) at 1200 °C, 1300 °C, 1400 °C and 1500 °C, respectively. For the flame spheroidization method, the sintered powders were sprayed into a water-filled metal container using an oxygen-acetylene gun (Metco 9M, Oerlikon Metco, Switzerland) at the stand-off distance of 40 cm. The parameters were shown in Table 1. Then, the water was evaporated at 100 °C; and the powder was sieved by 150 mesh.

Table 1. Parameters used in plasma treatment.

Spray Current/A	Spray Voltage/V	Flow Rate of Primary Gas/SCFH *	Flow Rate of Carrier Gas/SCFH	Powder Giving Rate/g/min	Spray Distance/cm
550	55	120	12	20	40

* SCFH, standard cubic foot per hour. 1SCFH = 0.472 L min^{-1}.

The mullite/Si coating was thermal sprayed with an APS torch (Metco 9M) onto the SiC substrates, and the parameters are shown in Table 2.

Table 2. Parameters of APS mullite/Si coating.

	Spray Current/A	Spray Voltage/V	Flow Rate of Primary Gas/SCFH	Flow Rate of Carrier Gas/SCFH	Powder Giving Rate/g/min	Spray Distance/cm
Si	450	45	80	12	35	12
mullite	550	55	120	12	35	12

2.3. Characterization Methods

The microstructures of different particles were detected by the scanning electron microscopy (SEM; SS-550 Shimadzu, Kyoto, Japan) equipped with an energy-dispersive X-ray spectroscopy (EDS), and the transmission electron microscopy (TEM; JEOL 2100, Tokyo, Japan).

The bulk density, tap density and repose angle of the particle were determined by a densimeter (BT-1000, Dandong, China). The total time for 50 g powders to fully flow out of the container is the flowability of the powders.

Particle size distributions of spray-dried and sintering powders were determined with a laser diffraction analyzer (Easysizer 2.0, OMEC, Zhuhai, China).

The TG-DTA was performed with Simultaneous Thermal Analyzer of Netzh, model STA 449 F3 (Bayern, Germany), at a heating rate of 10 °C/min, using alumina standard.

Phase analysis was performed using an X-ray diffractometer (XRD-6000, Shimadzu, Tokyo, Japan) with a θ/2θ configuration, in the 2θ range of 10–90°, with 0.0165° steps.

The total porosity (%) of different layers of EBCs was determined by microstructure image processing (MIP) software.

3. Results and Discussion

3.1. Characteristic of Spray-Dried Powders

Figure 1 shows the morphology of spray-dried powders. It can be seen that the granulating powders have good sphericity and smooth surface. They displayed typical characteristics of spray granulation powders.

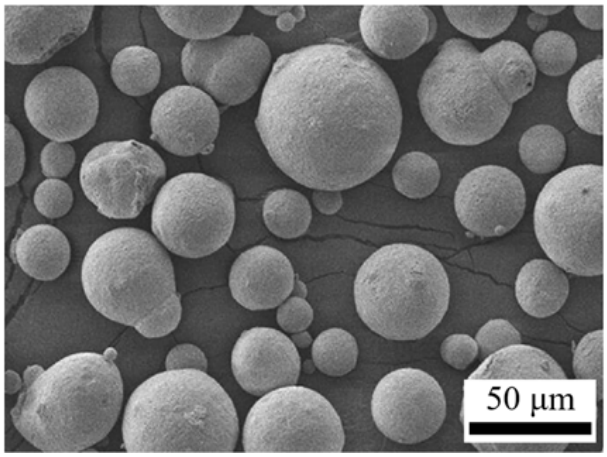

Figure 1. Surface morphology of spray granulation powders.

Due to the fine grain size and large specific surface area, the sintering activity of nanostructured powders was higher than that of traditional micrometer powders. In this study, thermal gravity-differential thermal analysis (TG−DTA) of the powders after spray drying was used to determine the reaction temperature, as can be seen in Figure 2. As can be seen from the TG curve, there was about 2.7% mass loss from room temperature (RT) to 550 °C, which is due to the evaporation of water and the decomposition of PVA. The absorption peaks at 119 °C and 356 °C in DTA curve represented the evaporation of water and the decomposition of PVA. No obvious mass change happened in the range of 500–1400 °C. The DTA curve shows an apparent exothermic phenomenon corresponds to the peaks at 1142 °C and 1344 °C, respectively. The exothermic peak of 1142 °C corresponds to the starting reaction temperature [33,34]. The exothermic peak of 1344 °C indicated the violent reaction of Al_2O_3 and SiO_2. The synthesis temperature of mullite was around 1344 °C.

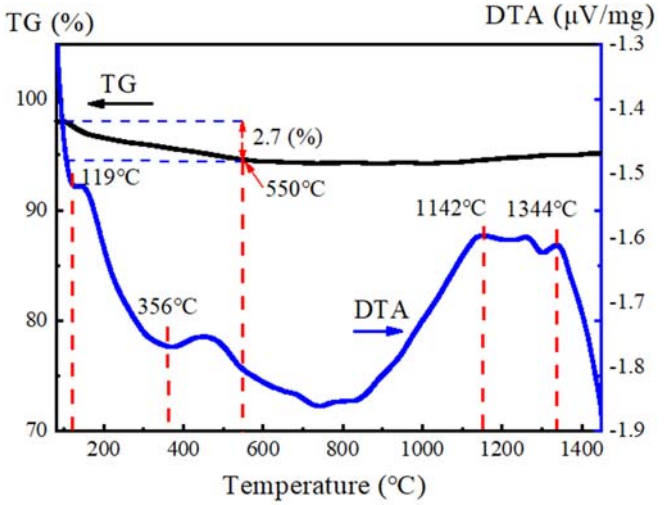

Figure 2. TG−DTA curve of spray granulation powders.

As can be seen in Figure 3, the peaks of mullite, Al_2O_3 and SiO_2 can be detected at 1200 °C, showing that the reaction of the Al_2O_3 and SiO_2 is not enough. The content of mullite increased significantly with the increase of the temperature. When the temperature reached 1500 °C, no amorphous and secondary phases were observed. This indicated the reaction of the Al_2O_3 and SiO_2 was fully completed. A typical mullite structure was observed, and the structure of the powders was in agreement with the results reported by E. Garcia et al. [14].

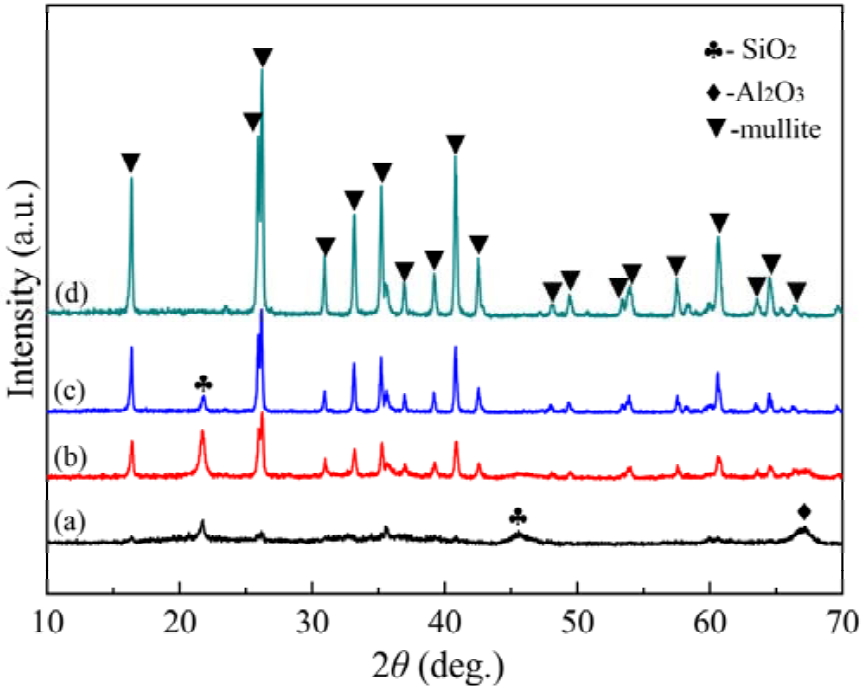

Figure 3. XRD patterns of spray granulation powders by different sintering temperatures for 2 h: (**a**) 1200 °C, (**b**) 1300 °C, (**c**) 1400 °C, and (**d**) 1500 °C.

The synthesized temperature of nanostructured mullite is lower than the Al_2O_3-SiO_2 eutectic temperature (~1590 °C) [35]. The mullitization temperature for the solid-state reaction between Al_2O_3 and SiO_2 can be higher than 1650 °C [36], though some chemical synthetic methods can be used to prepare reactive mullite powders, the reaction temperature of mullite ceramics was higher than 1600 °C [33]. The nanostructured mullite prepared by nanoparticle regranulation technology has effectively reduced the solid-phase sintering temperature.

The distribution of particle size for the powders at different sintering temperatures was shown in Figure 4. As the sintering temperature increased, the distribution range of the particle size for the spray granulated powder became narrowed. There was almost no change after 1300 °C, which indicated the sintering reaction was sufficient at 1300 °C. This result was consistent with the TG-DTA and XRD analysis. The D_{50} of granulated powders sintered at 1300–1500 °C were approximate 60 μm.

The density and flowability of powders at different sintering temperatures were shown in Table 3. The density and flowability of powders increased with the increase of temperature. The bulk density of powders increased from 0.81 g/cm^3 to 1.07 g/cm^3 while the tap density increased from 1.03 g/cm^3 to 1.26 g/cm^3. The repose angle reduced from 32° to 30°. The flowability increased from 222.2 s/50 g to 123.5 s/50 g. With the processing of sintering reaction, the growth of grain resulted in the decrease of voids between different particles. As a result, the particles became dense, thereby facilitating the flow of powders. Properly increasing sintering temperature was beneficial to improve the properties of feedstocks. However, sintering temperature should not be too high to avoid abnormal grain growth in order to obtain nanostructured feedstocks.

Table 3. Density and flowability powders prepared with different sintering temperatures.

T (°C)	Bulk Density (g/cm^3)	Tap Density (g/cm^3)	The Angle of Repose (°)	Flowability (s/50 g)
1200	0.81	1.03	32	222.2
1300	0.87	1.11	32	192.3
1400	0.96	1.15	30	159.6
1500	1.07	1.26	30	123.5

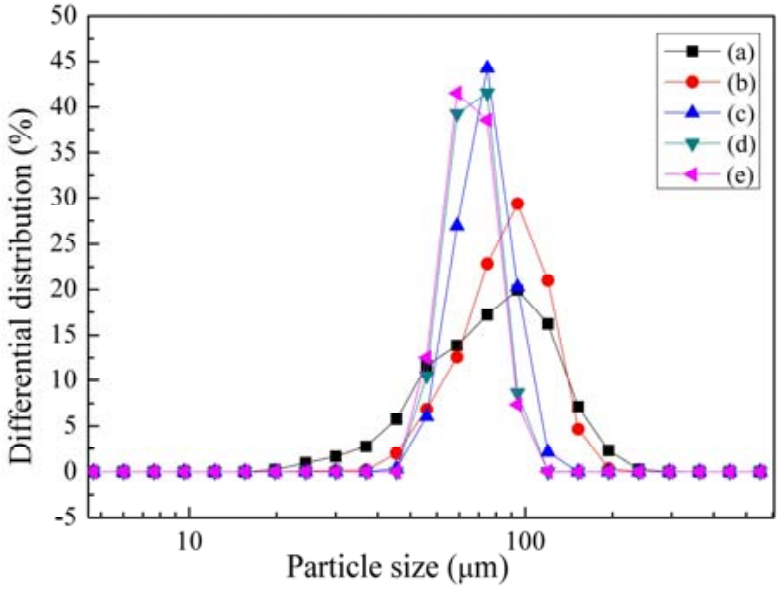

Figure 4. Particle size distribution of granulation powders at different sintering temperatures: (**a**) as-synthesized, (**b**) 1200 °C for 2 h, (**c**) 1300 °C for 2 h, (**d**) 1400 °C for 2 h, and (**e**) 1500 °C for 2 h.

Nanostructured powders are the basis of preparation of high-performance ceramic coatings. To confirm that the sintered powders were nanostructured, the average grain sizes of sintered mullite powders were determined by their XRD patterns and the Scherrer equation [37,38]. As can be seen in Table 4, the grain sizes at different sintering temperatures were in nano-scale. The grain size was 52 nm at 1500 °C. The comprehensive properties of coatings depend on the composition, microstructure, density and flowability of feedstocks. The mullite powders sintered at 1500 °C have nanostructure and the best flowability. Therefore, it is suitable for preparation of nanostructured EBCs by plasma spraying.

Table 4. Crystallite sizes of sintering powders with different temperatures.

T (°C)	1200	1300	1400	1500
Grain size (nm)	18	19	43	52

3.2. Characterization of Flame Spheroidized Powders

In order to facilitate thermal spraying, flame spheroidization process was used to further enhance the flowability and density of the powder. A proportion of the granules were sintered at 1500 °C for 2 h before the flame spheroidization treatment. The microstructure and cross-section morphology were shown in Figures 5 and 6. The micrographs of flame spheroidization mullite powders show the granule surfaces appeared smooth and dense. In the flame spheroidization process, the powder melted into liquid droplets under the plasma heat source. Under the protection of argon atmosphere, the small liquid droplets cooled rapidly and solidified into a spherical powder due to surface tension. This flame spheroidization process improved the density of the powders significantly. It indicated sphericity of the granules was improved after flame spheroidization treatment. The EDS

analysis (Figure 5b) indicated that the elements of Al, Si and O were uniformly distributed on the surface of the particles. The energy spectrum element analysis of the powder was shown in Figure 5b. It can be seen that the content of Al, Si, O elements was equivalent to the stoichiometric ($3Al_2O_3 \cdot 2SiO_2$) composition of mullite.

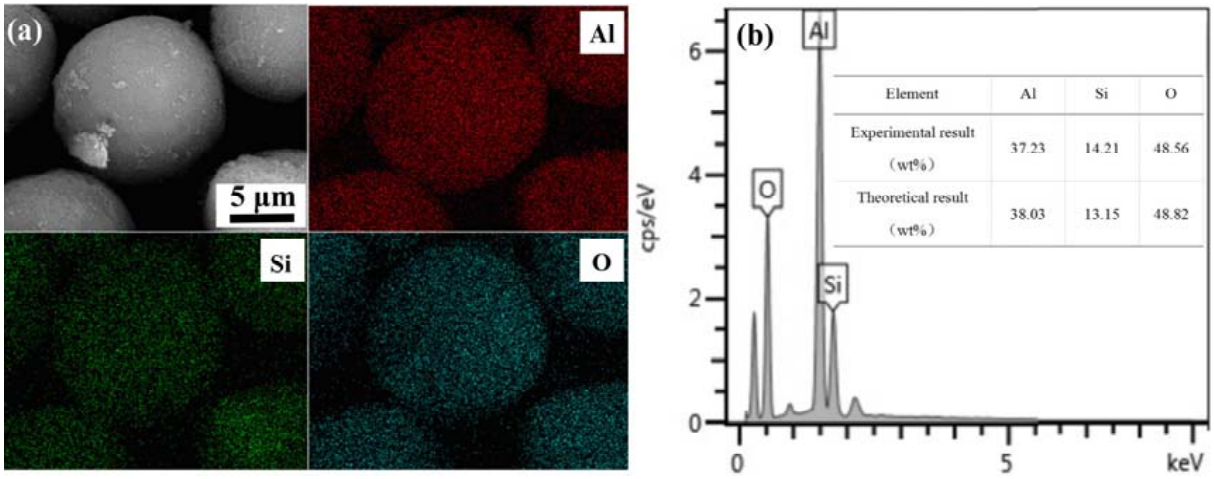

Figure 5. (**a**) SEM image and elemental distribution map of flame spheroidized mullite powders, (**b**) EDS spectrum corresponding to (**a**).

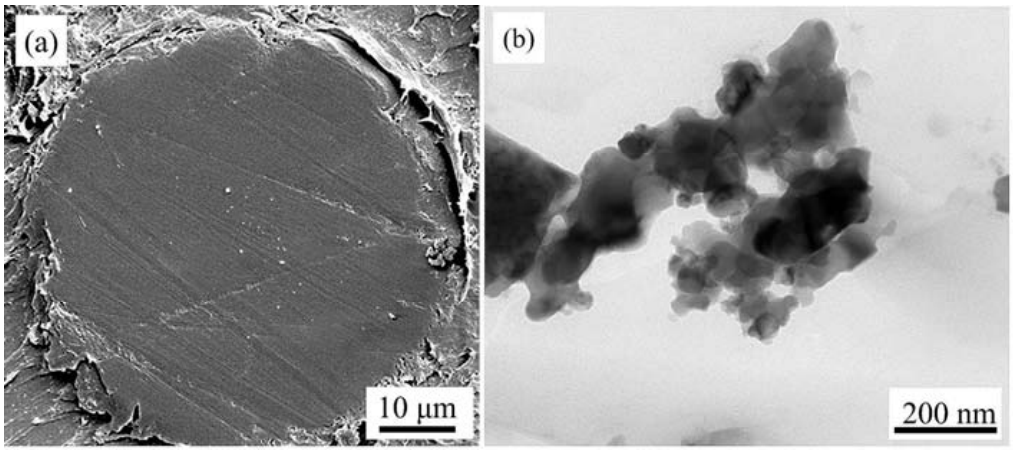

Figure 6. (**a**) Cross-section image of a flame spheroidized mullite, (**b**) TEM image of flame spheroidized powders.

Figure 6a displays the cross-section morphology of a particle of the mullite powder. No hole was observed in the polished cross-section and the structure was dense. In order to investigate the grain size of powders after flame spheroidization process, the feedstocks were dispersed before TEM analysis. The results of TEM analysis are shown in Figure 6b. It can be seen in Figure 6b, the grain size of feedstocks after flame spheroidization process was still nanostructured.

Figure 7 presented the XRD patterns of flame spheroidization mullite powders. The sharp and intense peaks on the XRD patterns were characteristic of mullite, which indicated that the powders were fully crystallized by the flame spheroidization method. This is because the process from melting to solidification of powder particles is very short in the flame spheroidization process. The flame spheroidization process is the reconstruction of powder particles without changing the original organization. Therefore, there is no disappearance of old phases and the appearance of new phases.

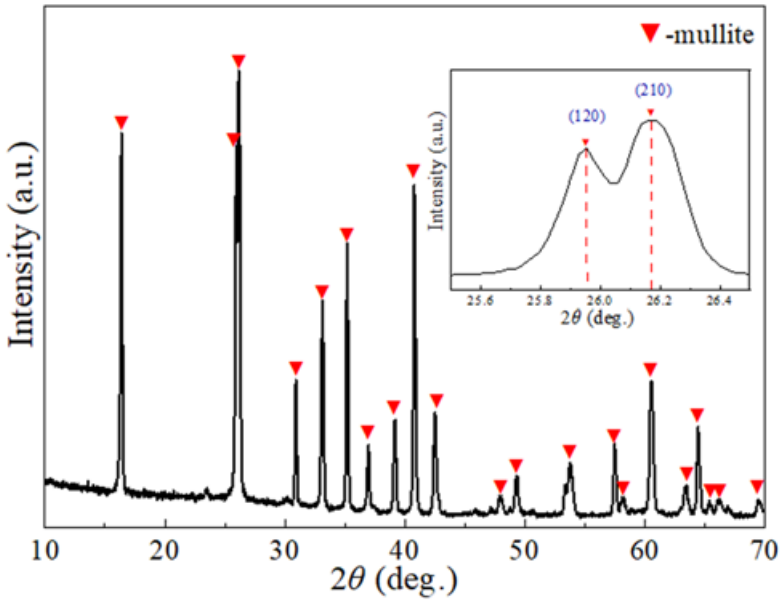

Figure 7. XRD pattern of flame spheroidized powders.

Two diffraction peaks, at the angle range of 25.5–26.5° in the pattern of flame spheroidization mullite, were in accord with the XRD patterns of JCPDF 79-1456. The two diffraction peaks were indexed on an orthorhombic lattice as (120) and (210). According to the XRD patterns of (210) lattice, the Debye–Scherrer equation was used to calculate the grain size of flame spheroidization mullite powders. The average grain sizes of flame spheroidization mullite powders were approximate 48 nm. The bulk density was 1.21 g/cm^3 and flowability was 88.7 s/50 g (Table 5), which is superior to the characteristics of sintering feedstocks. The results indicated that the physical properties of flame spheroidization feedstocks, such as flowability and density, have been greatly improved. In the plasma spraying process, the heat is easily transmitted into the powder due to the high bulk density of the flame spheroidization mullite feedstocks. As a result, the flame spheroidization mullite feedstocks will be heated and melted to form a dense coating structure. Therefore, the flame spheroidization treated nanostructured mullite feedstocks are more suitable for plasma spraying to prepare high-quality EBCs.

Table 5. Properties of flame spheroidized mullite powders.

Grain Size (nm)	Bulk Density (g/cm^3)	Tap Density (g/cm^3)	The Angle of Repose (°)	Flowability (s/50 g)
48	1.21	1.39	28	88.7

3.3. Phase Composition of Mullite Coating

Nanostructured mullite coating was successfully prepared by plasma spraying with flame spheroidized mullite powders. Figure 8 shows the XRD pattern of as-sprayed mullite coating. As can be seen from the figure, the as-sprayed mullite coating exhibited a high degree of crystallinity, which was beneficial to improve the thermal shock resistance and adhesion of the coating [13]. The average grain size of the mullite coating was 35 nm, which was determined from Figure 8 by using the Scherrer equation. This indicated the mullite coating was nanostructured. The rapid melting and solidification in the plasma spraying process decreased the grain size of the coating.

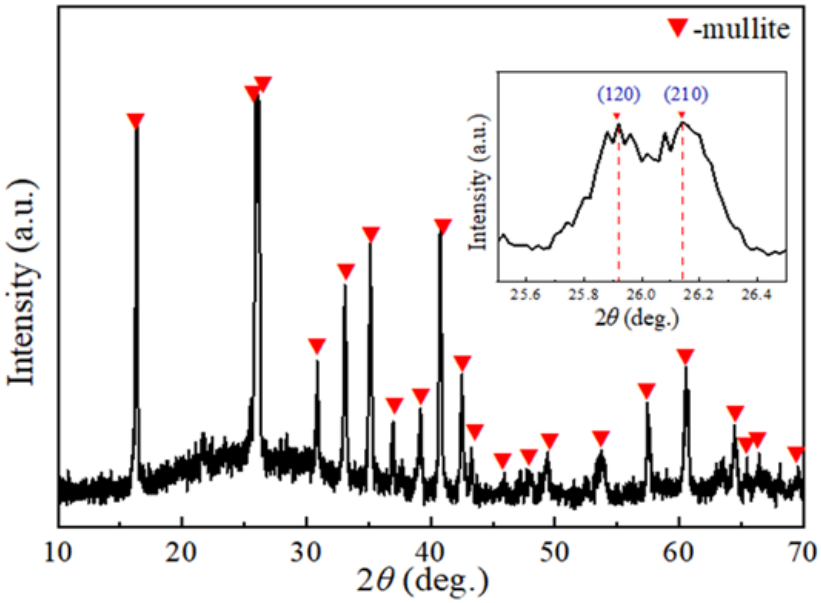

Figure 8. XRD pattern of as-sprayed mullite coating.

3.4. Morphology of Nanostructured Environmental Barrier Coating

Figure 9 depicted the cross-sectional morphologies of the as-sprayed coating. It showed typical bi-layer coating structure. The top mullite layer was a continuous layer (with 60–80 μm thickness). It can be seen that the mullite/Si coating exhibited good bonding. The different layers can be distinguished by observing the distribution of Al, Si elements in the coating. All elements in the coating were evenly distributed. The Si layer appeared dense and almost no visible pores, which combined with the substrate closely.

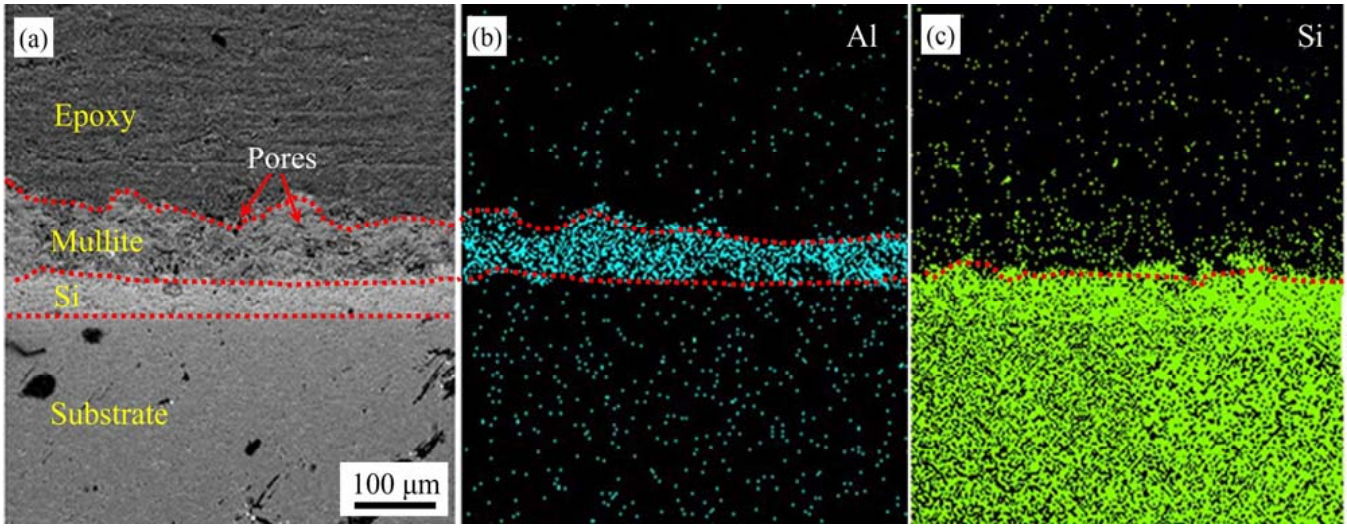

Figure 9. (**a**) Cross-section of as-sprayed EBC, (**b**) element distribution map of Al, and (**c**) element distribution map of Si.

No crack was found in the nanostructured mullite coating. This is because the flowability of the feedstocks is good and the distribution of particle size is uniform, which results in the melting of the feedstocks is relatively uniform in the plasma spraying process. Therefore, the residual stress in the coating after the spraying is relatively small. There are some tiny closed pores in the coating, which was caused by the unmelted nanoparticles. The interior structure of the nano zone was beneficial to the corrosion resistance, because the water vapor and CMAS cannot penetrate into the layer. The small closed pores can

enhance phonon scattering, reduce thermal diffusivity, relieve the stress of the coating, and improve the toughness and its thermal shock resistance [39,40].

Image-Pro Plus software was used to process the coating cross-section SEM images and calculate their corresponding porosities. Table 6 showed the porosities and cracks of mullite layers prepared by different feedstocks. The porosity of nanostructured mullite coating is 6.5%, which indicated that the coating has high density. The reason for the high density of the nanostructured mullite coating can be attributed to two aspects. On the one hand, the density of the spraying feedstocks after flame spheroidization treatment is very high. No pores were detected on the surface and inside of the mullite powders. On the other hand, the particles impact the underlying Si coating at high speed during the plasma spraying process, resulting in the spherical particles transforming into flat particles. The high flatness of the particles is beneficial to the melting of the nanoparticles by the plasma flame. Therefore, the porosity of the coating is significantly reduced.

Table 6. The cracks and porosities of mullite layers by APS prepared by different feedstocks.

Contribution	Layer Thickness (μm)	Porosity (%)	Crack	References
Nanostructured mullite	60	6.5	No cracks	This work
Fused or sintered mullite purchased from commercial vendors	200–400	Obvious porosity	Obvious cracks	K.N. Lee et al. [13].
#1020 mullite, d_{50} 30 μm (Saint-Gobain, Worchester, MA, USA)	50	11	No cracks in mullite coating, 15 vertical cracks/cm in BSAS layer (BSAS/mullite/Si)	V. Cojocaru et al. [15].
1–49 mullite powder (Praxair Wiggensbach, Germany)	800/150	Not mention	Through-thickness cracking 1.8–2.9 cracks/mm	S. Latzel et al. [20].
Spray-dried and freeze-granulated mullite (both are porous-type structure)	50–100	Spray-dried 9 and freeze-granulated 30	Periodically spaced vertical cracks	C.V. Cojocaru et al. [25].
Mullite powder, HC Stark, Karlsruhe, Germany	200	11	Through-thickness cracking between BSAS and mullite coating was evident (BSAS/mullite/Si)	B.J. Harder et al. [41].

Compared with the microstructured mullite layers, nanostructured mullite coating should display superior properties. Consequently, the nanostructured mullite coating has promising prospects in the next generation advanced EBCs.

4. Conclusions

(1) Nanostructured mullite spherical feedstocks were prepared by nanoparticle regranulation technology. The D_{50} of granulated powders sintered at 1300–1500 °C was approximate 60μm. The grain size was 52 nm at 1500 °C. The bulk density was 1.07 g/cm^3 with the flowability of 123.5 s/50 g, which is suitable for plasma spraying.

(2) The sintering temperatures have an obvious influence on the synthesis of nanostructured mullite. The formation of mullite started at 1200 °C. With the increase of the temperature, the diffraction peak of mullite enhanced. The reaction of Al_2O_3 and SiO_2 was fully completed at 1500 °C. The nanostructured mullite prepared by nanoparticle regranulation technology has effectively reduced the solid-phase sintering temperature.

(3) The flame spheroidization reduced the grain size of the nanostructured mullite. After flame spheroidization, the grain size of the spherical feedstocks was 48 nm. The flowability was 88.7 s/50 g and the bulk density was 1.21 g/cm^3. The flame spheroidized

nanostructured mullite feedstocks are more suitable for plasma spraying to prepare high-quality environmental barrier coatings.

(4) The grain size of mullite coating is 35 nm. The rapid melting and solidification in the plasma spraying process decreased the grain size of the coating. The porosity of nanostructured mullite coating was 6.5% and no crack was found. The high density of the nanostructured mullite coating can be attributed to the high density of the spraying feedstocks after flame spheroidization treatment, and the nanostructured mullite particles impact the underlying Si coating at high speed during plasma spraying process. A small amount of tiny closed pores in the coating were beneficial to the corrosion resistance of the coating. The nanostructured mullite coating has promising prospects in the next generation advanced environmental barrier coatings.

Author Contributions: Conceptualization, X.Z.; methodology, J.J.; validation, X.Z., F.X. and X.G.; investigation, L.W.; resources, M.Y.; data curation, S.L.; writing—original draft preparation, F.X.; writing—review and editing, X.G.; funding acquisition, Y.W. All authors have read and agreed to the published version of the manuscript.

Funding: This research was funded by National Science and Technology Major Project (No. 2017-VI-0020-0093), National Key Research and Development Project (No. 2020YFB2007900), Open Foundation from National Key Laboratory of Materials Behavior and Evaluation Technology in Space Environments, National Natural Science Foundation of China (No. 52001217) and Doctoral Start-up Foundation of Liaoning Province (No. 2021-BS-195).

Institutional Review Board Statement: Not applicable.

Informed Consent Statement: Not applicable.

Data Availability Statement: Not applicable.

Conflicts of Interest: The authors declare no conflict of interest.

References

1. Lee, K.N. Current Status of Environmental Barrier Coatings for Si-Based Ceramics. *Surf. Coat. Technol.* **2000**, *133–134*, 1–7. [CrossRef]
2. Basu, S.N.; Sarin, V.K. Thermal and Environmental Barrier Coatings for Si-Based Ceramics. *Compr. Hard Mater.* **2014**, *2*, 469–489.
3. Ramasamy, S.; Tewari, S.N.; Lee, K.N.; Bhatt, R.T.; Fox, D.S. Slurry Based Multilayer Environmental Barrier Coatings for Silicon Carbide and Silicon Nitride Ceramics—I. Processing. *Surf. Coat. Technol.* **2010**, *205*, 258–265. [CrossRef]
4. Bhatt, R.T.; Choi, S.R.; Cosgriff, L.M.; Fox, D.S.; Lee, K.N. Impact Resistance of Environmental Barrier Coated SiC/SiC Composites. *Mater. Sci. Eng. A* **2008**, *476*, 8–19. [CrossRef]
5. Eaton, H.E.; Linsey, G.D. Accelerated Oxidation of SiC CMC's by Water Vapor and Protection via Environmental Barrier Coating Approach. *J. Eur. Ceram. Soc.* **2002**, *22*, 2741–2747. [CrossRef]
6. Ueno, S.; Ohji, T.; Lin, H.T. Corrosion and Recession of Mullite in Water Vapor Environment. *J. Eur. Ceram. Soc.* **2008**, *28*, 431–435. [CrossRef]
7. Stolzenburg, F.; Kenesei, P.; Almer, J.; Lee, K.N.; Johnson, M.T.; Faber, K.T. The Influence of Calcium- Magnesium-Aluminosilicate Deposits on Internal Stresses in $Yb_2Si_2O_7$ Multilayer Environmental Barrier Coatings. *Acta Mater.* **2016**, *105*, 189–198. [CrossRef]
8. Bakan, E.; Marcano, D.; Zhou, D.; Sohn, Y.J.; Mauer, G.; Vaßen, R. $Yb_2Si_2O_7$ Environmental Barrier Coatings Deposited by Various Thermal Spray Techniques: A Preliminary Comparative Study. *J. Therm. Spray Technol.* **2017**, *26*, 1011–1024. [CrossRef]
9. Chen, H.; Zhang, C.; Liu, Y.-C.; Song, P.; Li, W.-X.; Yang, G.; Liu, B. Recent progress in thermal/environmental barrier coatings and their corrosion resistance. *Rare Met.* **2020**, *5*, 498–512. [CrossRef]
10. Laura, R.T.; Nitin, P.P. Towards multifunctional thermal environmental barrier coatings (TEBCs) based on rare-earth pyrosilicate solid-solution ceramics. *Scripta Mater.* **2018**, *154*, 111–117.
11. Botero, C.A.; Jimenez-Pique, E.; Martin, R.; Kulkarni, T.; Sarin, V.K.; Llanes, L. Influence of Temperature and Hot Corrosion on the Micro-Nanomechanical Behavior of Protective Mullite EBCs. *Int. J. Refract. Met. Hard Mater.* **2015**, *49*, 383–391. [CrossRef]
12. Price, J.R.; van Roode, M.; Stala, C. Ceramic Oxide-Coated Silicon Carbide for High Temperature Corrosive Environments. *Key Eng. Mater.* **1992**, *72*, 71–84. [CrossRef]
13. Lee, K.N.; Miller, R.A.; Jacobson, N.S. New Generation of Plasma-Sprayed Mullite Coatings on Silicon Carbide. *J. Am. Ceram. Soc.* **1995**, *78*, 705–710. [CrossRef]
14. Garcia, E.; Mesquita-Guimaraes, J.; Miranzo, P.; Osendi, M.I.; Wang, Y.; Lima, R.S.; Moreau, C. Mullite and Mullite/ZrO_2-7wt.%Y_2O_3 Powders for Thermal Spraying of Environmental Barrier Coatings. *J. Therm. Spray Technol.* **2010**, *19*, 286–293. [CrossRef]

15. Cojocaru, C.V.; Levesque, D.; Moreau, C.; Lima, R.S. Performance of Thermally Sprayed Si/Mullite/BSAS Environmental Barrier Coatings Exposed to Thermal Cycling in Water Vapor Environment. *Surf. Coat. Technol.* **2013**, *216*, 215–223. [CrossRef]
16. Garcia, E.; Mesquita-Guimaraes, J.; Miranzo, P.; Osendi, M.I. Crystallization Studies in Mullite and Mullite-YSZ Beads. *J. Eur. Ceram. Soc.* **2010**, *30*, 2003–2008. [CrossRef]
17. Mah, T.I.; Mazdiyasni, K.S. Mechanical Properties of Mullite. *J. Am. Ceram. Soc.* **2010**, *66*, 699–703. [CrossRef]
18. Hamidouche, M.; Bouaouadja, N.; Olagnon, C.; Fantozzi, G. Thermal shock behaviour of mullite ceramic. *Ceram. Int.* **2003**, *29*, 599–609. [CrossRef]
19. Lee, K.N.; Miller, R.A. Development and Environmental Durability of Mullite and Mullite/YSZ Dual Layer Coatings for SiC and Si_3N_4 Ceramics. *Surf. Coat. Technol.* **1996**, *86*, 142–148. [CrossRef]
20. Latzel, S.; VaBen, R.; Stover, D. New Environmental Barrier Coating System on Carbon-Fiber Reinforced Silicon Carbide Composites. *J. Therm. Spray Technol.* **2005**, *14*, 268–272. [CrossRef]
21. Mesquita-Guimaraes, J.; García, E.; Miranzo, P.; Osendi, M.I.; Cojocaru, C.V.; Lima, S.R. Mullite-YSZ Multilayered Environmental Barrier Coatings Tested in Cycling Conditions under Water Vapor Atmosphere. *Surf. Coat. Technol.* **2012**, *209*, 103–109. [CrossRef]
22. Nasiri, N.A.; Patra, N.; Horlait, D.; Jayaseelan, D.D.; Lee, W.E. Thermal Properties of Rare-Earth Monosilicates for EBC on Si-Based Ceramic Composites. *J. Am. Ceram. Soc.* **2016**, *99*, 589–596. [CrossRef]
23. Harder, B.J.; Zhu, D.; Schmitt, M.P.; Wolfe, D.E. Microstructural Effects and Properties of Non-line-of-Slight Coating Processing via Plasma Spray-Physical Vapor Depositon. *J. Therm. Spray Technol.* **2017**, *26*, 1052–1061. [CrossRef]
24. Li, J.F.; Liao, H.; Wang, X.Y.; Coddet, C.; Chen, H.; Ding, C.X. Plasma spraying of nanostructured partially yttria stabilized zirconia powders. *Thin Solid Film.* **2004**, *460*, 101–115. [CrossRef]
25. Cojocaru, C.V.; Wang, Y.; Moreau, C.; Lima, R.S.; Mesquita-Guimarães, J.; Garcia, E.; Miranzo, P.; Osendi, M.I. Mechanical Behavior of Air Plasma-Sprayed YSZ Functionally Graded Mullite Coatings Investigated via Instrumented Indentation. *J. Therm. Spray Technol.* **2011**, *20*, 100–107. [CrossRef]
26. Xiao, J.; Liu, Q.; Li, J.; Guo, H.; Xu, H. Microstructure and High-Temperature Oxidation Behavior of Plasma-Sprayed Si/Yb_2SiO_5 Environmental Barrier Coatings. *Chin. J. Aeronaut.* **2019**, *32*, 1994–1999. [CrossRef]
27. Lima, R.S.; Kucuk, A.; Berndt, C.C. Evaluation of Microhardness and Elastic Modulus of Thermally Sprayed Nanostructured Zirconia Coatings. *Surf. Coat. Technol.* **2001**, *135*, 166–172. [CrossRef]
28. Ahmed, I.; Bergman, T.L. Thermal Modeling of Plasma Spray Deposition of Nanostructured Ceramics. *J. Therm. Spray Technol.* **1999**, *8*, 315–322. [CrossRef]
29. Zhu, Y.; Huang, M.; Huang, J.; Ding, C. Vacuum-Plasma Sprayed Nanostructured Titanium Oxide Films. *J. Therm. Spray Technol.* **1999**, *8*, 219–222. [CrossRef]
30. Wang, Y.; Jiang, S.; Wang, M.; Wang, S.; Xiao, T.D.; Strutt, P.R. Abrasive Wear Characteristics of Plasma Sprayed Nanostructured Alumina/Titania Coatings. *Wear* **2000**, *237*, 176–185. [CrossRef]
31. Wang, L.; Wang, Y.; Sun, X.G.; He, J.Q.; Pan, Z.Y.; Yu, L.L. Preparation and characterization of nanostructured $La_2Zr_2O_7$ feedstock used for plasma spraying. *Powder Technol.* **2011**, *212*, 267–277. [CrossRef]
32. Wang, Y.; Tian, W.; Yang, Y. Preparation and characterization of re modified nanocrystalline Al_2O_3/13wt%TiO_2 feedstock for plasma spraying. *J. Nanosci. Nanotechnol.* **2009**, *9*, 1445–1448. [CrossRef] [PubMed]
33. Imose, M.; Takano, Y.; Yoshinaka, M.; Hirota, K.; Yamaguchi, O. Novel Synthesis of Mullite Powder with High Surface Area. *J. Am. Ceram. Soc.* **1998**, *81*, 1537–1540. [CrossRef]
34. Gören, R.; Özgür, C. Rapid synthesis of mullite powders. *J. Ceram. Process. Res.* **2012**, *13*, 262–266.
35. Klug, F.J.; Prochazka, S. Alumina-Silica Phase Diagram in the Mullite Region. *J. Am. Ceram. Soc.* **1987**, *70*, 750–759. [CrossRef]
36. Vargas, F.; Restrepo, E.; Rodriguez, J.E.; Vargas, F.; Arbelaez, L.; Caballero, P.; Arias, J.; Lopez, E.; Latorre, G.; Duarte, G. Solid-state synthesis of mullite from spent catalysts for manufacturing refractory brick coatings. *Ceram. Int.* **2018**, *44*, 3556–3562. [CrossRef]
37. He, K.; Chen, N.; Wang, C.; Wei, L.; Chen, J. Method for Determining Crystal Grain Size by X-ray Diffraction. *Cryst. Res. Technol.* **2018**, *53*, 1700157. [CrossRef]
38. Uvarov, V.; Popov, I. Metrological Characterization of X-ray Diffraction Methods at Different Acquisition Geometries for Determination of Crystallite Size in Nano-Scale Materials. *Mater. Charact.* **2013**, *85*, 111–123. [CrossRef]
39. Zhou, F.; Wang, Y.; Liu, M.; Deng, C.; Li, Y.; Wang, Y.; Zhang, X. Bonding strength and thermal conductivity of novel nanostructured $La_2(Zr_{0.75}Ce_{0.25})_2O_7$/8YSZ coatings. *Appl. Surf. Sci.* **2019**, *481*, 460–465. [CrossRef]
40. Guo, H.B.; Murakami, H.; Kuroda, S. Microstructures and properties of plasma sprayed segmented thermal barrier coatings. *J. Am. Ceram. Soc.* **2006**, *89*, 1432–1439. [CrossRef]
41. Harder, B.J.; Almer, J.D.; Weyant, C.M.; Lee, K.N.; Faber, K.T. Residual Stress Analysis of Mullite Environmental Barrier Coatings. *J. Am. Ceram. Soc.* **2009**, *92*, 452–459. [CrossRef]